nature energy

SUPPLEMENTARY INFORMATION

ARTICLE NUMBER: 17053 | DOI: 10.1038/NENERGY.2017.53

In the format provided by the authors and unedited.

# *Intrinsic Non-Radiative Voltage Losses in Fullerene-Based Organic Solar Cells*

Johannes Benduhn[1,*], Kristofer Tvingstedt[2,*], Fortunato Piersimoni[3], Sascha Ullbrich[1], Yeli Fan[4,‡], Manuel Tropiano[5], Kathryn A. McGarry[6], Olaf Zeika[1], Moritz K. Riede[7], Christopher J. Douglas[6], Stephen Barlow[4], Seth R. Marder[4], Dieter Neher[3], Donato Spoltore[1], Koen Vandewal[1,*]

* Corresponding authors (johannes.benduhn@iapp.de, ktvingstedt@physik.uni-wuerzburg.de, koen.vandewal@iapp.de)

[1] Dresden Integrated Center for Applied Physics and Photonic Materials (IAPP) and Institute for Applied Physics, Technische Universität Dresden, Nöthnitzer Str. 61, 01187 Dresden, Germany

[2] Experimental Physics VI, Julius-Maximilian University of Würzburg, 97074 Würzburg, Germany

[3] Institute of Physics and Astronomy, University of Potsdam, Karl-Liebknecht-Str. 24-25, 14476 Potsdam, Germany

[4] Center for Organic Photonics and Electronics and School of Chemistry and Biochemistry, Georgia Institute of Technology, Atlanta, Georgia 30332-0400, United States

[5] Chemistry Research Laboratory, University of Oxford, Mansfield Road, Oxford OX1 3TA, United Kingdom

[6] Department of Chemistry, University of Minnesota, 207 Pleasant St SE, Minneapolis, 55455, United States

[7] Department of Physics, University of Oxford, Parks Road, Oxford OX1 3PU, United Kingdom

‡ Current address: School of Chemistry and Chemical Engineering, Southeast University, Nanjing 211189, Jiangsu, P.R. China

# Supplementary Notes

## Supplementary Notes 1 - Theory of Voltage Losses

At open circuit, we assume detailed balance of generation ($G$) and recombination ($R$) rate ($G = R$), where all the recombination takes place via CT states:

$$G = kN_{\mathrm{CT}}\ , \tag{1}$$

where $k$ is the total recombination rate constant which is the sum of the radiative and the non-radiative recombination rate[1]. $N_{\mathrm{CT}}$ is the density of populated CT states which can be described by:

$$N_{\mathrm{CT}} = N_{\mathrm{CTC}}\exp\left(\frac{-E_{\mathrm{CT}}+qV_{\mathrm{OC}}}{k_{\mathrm{B}}T}\right), \tag{2}$$

with $N_{\mathrm{CTC}}$ as the density of CT states. Hereby, we assume in Supplementary Equation (1) that $k$ is constant, implying that higher orders of recombination are neglected. The fact that the ideality for most of the studied systems was found to be close to unity, supports this assumption (see Supplementary Figure 1).

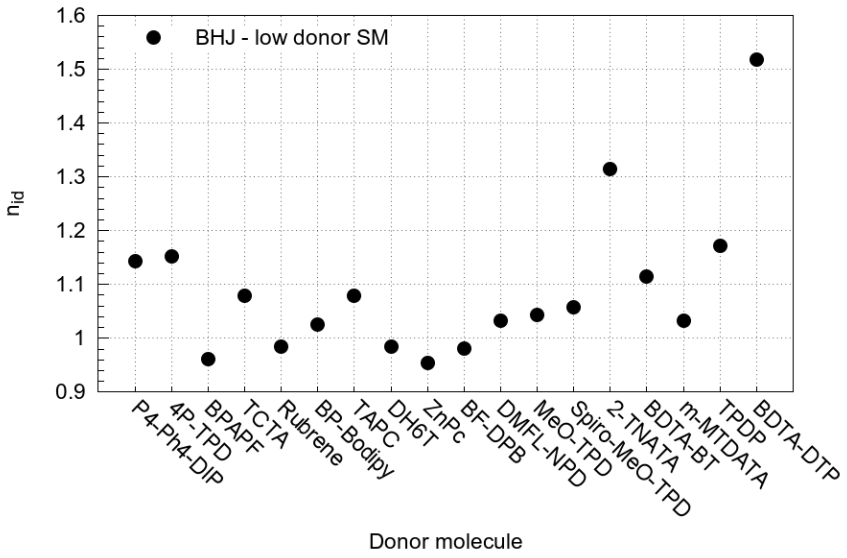


**Supplementary Figure 1 | Ideality Factor $n_{id}$.** Ideality factor of selected low donor OSCs compromised of 94 mol% of $C_{60}$ and the noted donor molecule. The donor molecules are sorted with respect to the magnitude of the $E_{CT}$ of the OSC, the highest $E_{CT}$ is on the left side.

In OSCs, the non-radiative recombination rate is much larger than the radiative one. The recently highest reported $EQE_{EL}$ for OSCs is about $10^{-4}$ [2].

$$k = k_{\mathrm{r}} + k_{\mathrm{nr}} \approx k_{\mathrm{nr}} \tag{3}$$

By rearranging Supplementary Equation (2), we get a relation for the $V_{OC}$:

$$qV_{OC} = E_{CT} + k_B T \ln\left(\frac{G}{k\, N_{CTC}}\right). \quad (4)$$

We identify the second term on the right side of Supplementary Equation (4) to the overall voltage losses ($\Delta V_{OC}$) with respect to $E_{CT}$:

$$\Rightarrow \Delta V_{OC} = \frac{k_B T}{q} \ln\left(\frac{(k_r + k_{nr})\, N_{CTC}}{G}\right) = V_{OC} - \frac{E_{CT}}{q}. \quad (5)$$

Furthermore, we can split $\Delta V_{OC}$ into radiative ($\Delta V_r$) and non-radiative voltage losses ($\Delta V_{nr}$):

$$q\,\Delta V_{OC} = k_B T \ln\left(\frac{k_r}{k_r}\frac{(k_r + k_{nr})\, N_{CTC}}{G}\right), \quad (6)$$

$$q\,\Delta V_{OC} = k_B T \ln\left(\frac{k_r + k_{nr}}{k_r}\right) + k_B T \ln\left(\frac{k_r N_{CTC}}{G}\right) = q\,\Delta V_{nr} + q\,\Delta V_r. \quad (7)$$

From Supplementary Equation (7) we can summarize the following relations, see Supplementary Table 1.

**Supplementary Table 1 | Summary of Expressions for Voltage Losses in Excitonic SCs.** The $V_{OC}$ discussed in this paper refers, due the standard testing conditions of SCs, to an illumination of AM1.5G. $V_{OC,rad}$ equals the $V_{OC}$ if only radiative recombination would take place.

| Quantity | Definition by rates | Definition by SC characteristics |
|---|---|---|
| **Overall voltage losses** | $\Delta V_{OC} = \frac{k_B T}{q} \ln\left(\frac{(k_r + k_{nr})\, N_{CTC}}{G}\right)$ | $\Delta V_{OC} = E_{CT} - V_{OC} = \Delta V_r + \Delta V_{nr}$ |
| **Radiative voltage losses** | $\Delta V_r = \frac{k_B T}{q} \ln\left(\frac{k_r N_{CTC}}{G}\right)$ | $\Delta V_r = E_{CT} - V_{OC,rad}$ |
| **Non-radiative voltage losses** | $\Delta V_{nr} = \frac{k_B T}{q} \ln\left(\frac{k_r + k_{nr}}{k_r}\right)$ | $\Delta V_{nr} = V_{OC,rad} - V_{OC}$ |
| **Radiative efficiency** | $EQE_{EL} = \frac{k_r}{k_r + k_{nr}} \approx \frac{k_r}{k_{nr}}$ | $\Delta V_{nr} = \frac{k_B T}{q} \ln\left(\frac{1}{EQE_{EL}}\right)$ |

## Supplementary Notes 2 - Simple Derivation of the "Energy-Gap Law" for Non-Radiative Recombination

At open circuit, a formed charge-transfer state ($CT^1$) can recombine either radiatively ($k_r$) or non-radiatively ($k_{nr}$) to the ground state ($S_0$). Free charges can recombine only if they form a state which is coupled to the ground state, which is by definition a CT state[3, 4]. Here, other decay possibilities such as intersystem crossing ($k_{ISC}$) to the triplet-excited state ($T_1$) or a back transfer to the singlet-excited state ($S_1$) are considered not to play a major role in the overall recombination[5].

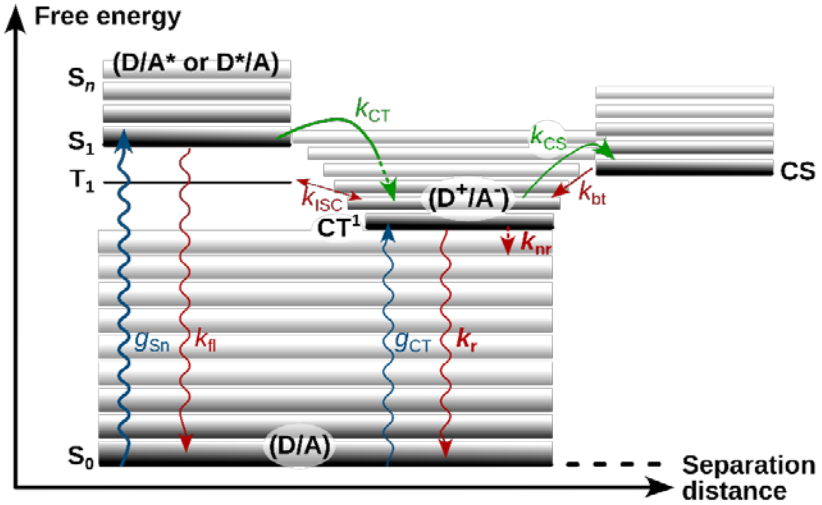


**Supplementary Figure 2 | Scheme of the Electronic Structure of a D-A System.** Upon an excitation of either the D or A ($g_{S1}$), the exciton can diffuse to the D-A interface where it creates a CT exciton. At open-circuit condition no charges (CS) are extracted, therefore, all charges have to recombine. This process is assumed to take place via the lowest energy state, the CT state, by radiative ($k_r$) and non-radiative ($k_{nr}$) recombination[1].

In what follows, we consider non-radiative decay from the CT state to the ground state as an electron transfer event, using Marcus theory and considering the presence of high frequency ($h\nu_v \approx k_B T$) and low frequency ($h\nu_s \ll k_B T$) vibrations. In electron transfer studies in solutions, the low frequency vibrations are referred to as solvent vibrations[6, 7], we attribute these vibrations to the deformation of the entire donor and acceptor molecule upon charging[8]. Since the energy spacing of these vibrations is very small, we can treat them classically[6, 7]. On the other hand, the high frequency vibrations represent skeletal vibrations, which are treated here with a mean vibrational mode ($\bar{\nu}_v$) to keep the description as simple as possible. An electron transfer from the excited state ($i$ = 0), the CT state, to the ground state ($j$) is proportional to the Franck-Condon overlap factor ($FC$), given by the sum of overlapping wave-functions of the CT state with all possible vibrational modes of the ground state ($j$ = {0, 1, 2,…})[9, 7]. Using the Franck-Condon theory thereby includes the Born-Oppenheimer approximation.

$$FC(g) = (4\pi\lambda_s k_B T)^{-1/2} \sum_{j=0}^{\infty} \frac{\exp(-S)\, S^j}{j!} \cdot \exp\left[-\frac{(g - j h\bar{\nu}_v - \lambda_s)^2}{4\lambda_s k_B T}\right]. \quad (8)$$

$S$ represents the ratio of the high frequency relaxation energy ($\lambda_v$) and the mean phonon-energy $h\bar{\nu}_v$ $\left(S = \frac{\lambda_v}{h\bar{\nu}_v}\right)$. The rate of non-radiative electron-transfer can be written as[7]:

$$k_{nr} = \frac{4\pi}{h} V^2 \, FC(g = E_{CT}) \,, \quad (9)$$

where *g* is the free energy for the non-radiative transition and equivalent to $E_{CT}$. To approximate the dependence of $k_{nr}$ on $E_{CT}$, we evaluate *FC*. First, we consider that the Gaussian term in Supplementary Equation (8) is maximal if *j* equals $j_{max}$.

$$E_{CT} - jh\bar{\nu}_{\nu} - \lambda_{s} = 0 \tag{10}$$

$$\Rightarrow j_{max} = \frac{E_{CT}-\lambda_{s}}{h\bar{\nu}_{\nu}} \tag{11}$$

The index $j_{max}$ clearly depends on $E_{CT}$. For typical values of $E_{CT}$, $\lambda_{s}$, and $h\bar{\nu}_{\nu}$ of our material system, we get $j = \{0.5 \dots 8\}$. We apply the Stirling approximation to evaluate the basic dependence of $\sum_{j=0}^{\infty} \frac{\exp(-S)\, S^{j}}{j!}$ on $E_{CT}$.

$$k_{nr} \propto \sum_{j=0}^{\infty} \frac{\exp(-S)\, S^{j}}{j!} \approx \sum_{j=0}^{\infty} \frac{\exp(-S)\, S^{j}}{\exp[\, j\ln(j) - j]} = \sum_{j=0}^{\infty} \exp[-S]\exp[j\ln(S)]\exp[-(j\ln(j) - j)] \tag{12}$$

Since the summand of *FC* with $j = j_{max}$ has the biggest contribution, we are going to consider only this term:

$$k_{nr} \propto \exp[-S]\exp[j_{max}\ln(S)]\exp[-(j_{max}\ln(j_{max}) - j_{max})] \tag{13}$$

$$\Rightarrow k_{nr} \propto \exp\left[j_{max}\left\{\ln\left(\frac{S}{j_{max}}\right) + 1\right\} - S\right] \tag{14}$$

$$\rightarrow k_{nr} \propto \exp\left[\frac{E_{CT}-\lambda_{s}}{h\bar{\nu}_{\nu}}\left\{\ln\left(\frac{\lambda_{\nu}}{E_{CT}-\lambda_{s}}\right) + 1\right\} - \frac{\lambda_{\nu}}{h\bar{\nu}_{\nu}}\right] \tag{15}$$

$$\rightarrow k_{nr} \propto \exp\left[-\frac{E_{CT}-\lambda_{s}}{h\bar{\nu}_{\nu}}\left\{\ln\left(\frac{E_{CT}-\lambda_{s}}{\lambda_{\nu}}\right) - 1\right\} - \frac{\lambda_{\nu}}{h\bar{\nu}_{\nu}}\right] . \tag{16}$$

To simplify *FC* to Supplementary Equation (16) we consider only the highest vibrational mode of the ground state, i.e. $j_{max}$, and we simplify the factorial of *j* as described in Supplementary Equation (12). Supplementary Figure 3 visualizes that these two approximations are very reasonable for further analyses.

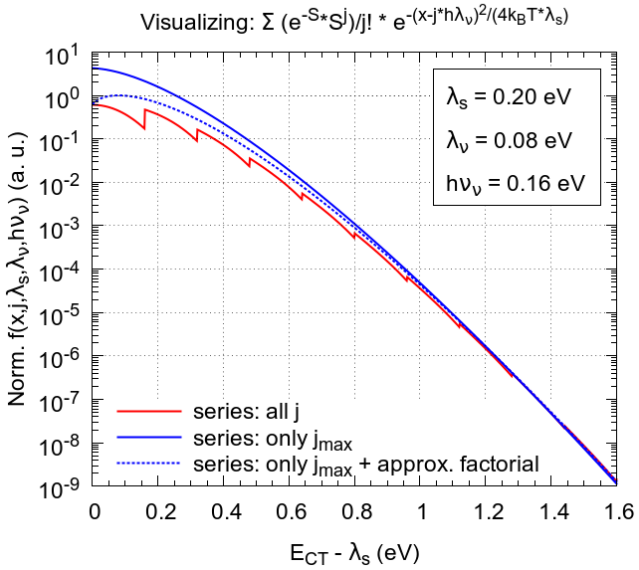


**Supplementary Figure 3 | Approximating the Franck-Condon Overlap Factor.** The Franck-Condon Overlap Factor in Supplementary Equation (8) is simplified by considering only the highest vibrational mode of the ground state, $j_{max}$, and approximating the factorial of $j$ as described in the text. As indicated by the dashed blue line, the approximations are reasonable.

According to Gould et al. 1993[7], we can express the radiative recombination rate constant as:

$$k_{\mathrm{r}} = \frac{64\pi^2}{3h^3c^3} n^3 \bar{\nu}_{\mathrm{v}} V^2 \, \Delta\, \mu^2 \,, \tag{17}$$

with $h\bar{\nu}_{\mathrm{v}} = E_{\mathrm{CT}} - \lambda_{\mathrm{s}} - \lambda_{\mathrm{v}}$. Here, $n$ is the refractive index of the material, $V$ is the matrix coupling element of both energy states, $\bar{\nu}_{\mathrm{v}}$ is the mean frequency of emission[7], and $\Delta\,\mu$ is the difference of the dipole moment of both energy states.

Since both the non-radiative and the radiative decay rate depend on the electronic coupling matrix, $k_{\mathrm{r}}, k_{\mathrm{nr}} \propto V^2$, we choose the quantity of the quantum efficiency of emission ($EQE_{\mathrm{EL}}$) which cancels out the dependency of the electronic coupling.

$$EQE_{\mathrm{EL}} \propto \frac{k_{\mathrm{r}}}{k_{\mathrm{r}}+k_{\mathrm{nr}}} \approx \frac{k_{\mathrm{r}}}{k_{\mathrm{nr}}} \tag{18}$$

Finally, with these approximations we get the following relation for the $EQE_{\mathrm{EL}}$:

$$EQE_{\mathrm{EL}} \propto \frac{\Delta\mu^2\,(E_{\mathrm{CT}}-\lambda_{\mathrm{s}}-\lambda_{\mathrm{v}})}{\exp\left[-\frac{E_{\mathrm{CT}}-\lambda_{\mathrm{s}}}{h\nu_{\mathrm{v}}}\left\{\ln\left(\frac{E_{\mathrm{CT}}-\lambda_{\mathrm{s}}}{\lambda_{\mathrm{v}}}\right)-1\right\}-\frac{\lambda_{\mathrm{v}}}{h\bar{\nu}_{\mathrm{v}}}\right]} \,. \tag{19}$$

We see that $EQE_{\mathrm{EL}}$ strongly scales with $E_{\mathrm{CT}} - \lambda_{\mathrm{s}}$. From the experimental point of view, the non-radiative voltage losses $\left(\Delta\, V_{\mathrm{nr}} = -\frac{k_{\mathrm{B}}T}{q}\ln(EQE_{\mathrm{EL}})\right)$ represent a fundamental important quantity, for which we find the following dependency:

$$\Rightarrow \Delta V_{nr} \propto -\frac{k_B T}{q} \cdot \left[\frac{E_{CT}-\lambda_s}{h\bar{\nu}_v}\left\{\ln\left(\frac{E_{CT}-\lambda_s}{\lambda_v}\right)-1\right\}+\frac{\lambda_v}{h\bar{\nu}_v}\right] \quad (20)$$

$$\Rightarrow \Delta V_{nr} \propto -\frac{k_B T}{q}\left[\frac{E_{CT}-\lambda_s}{h\bar{\nu}_v}\right] \quad (21)$$

Supplementary Equation (21) is a well know relation and in the literature and referred to as the "Energy-Gap law"[9, 7, 10, 11]. This approximation assumes that the difference of the dipole moments $\Delta\mu$, the relaxation energy of the high energy vibrations $\lambda_v$, and the typical mean phonon-energy of the high frequency vibrations $h\bar{\nu}_v$ are rather constant for all materials in this study. To visualize the impact of possible variations of these parameters, Supplementary Figure 4a-c shows a deviation of each parameter by a factor of 2. The black line shows the reciprocal of Supplementary Equation (19), with $x = E_{CT}$-$\lambda_s$, which describes the physical model the best, the grey area indicates a deviation of the black line by ±25 mV, assuming room temperature. The red solid line is a corresponding exponential fit of Supplementary Equation (19) which is very reasonable in the domain of $x$-values used in this study. A variation of $\Delta\mu$ would lead only to a relatively small vertical deviation, however, the slope of the relation does not change as shown by Supplementary Figure 4a. If $\lambda_v$ would change by a factor 2, especially higher $x$-values would be influenced and the slope would deviate by ~30%, see Supplementary Figure 4b. A deviation in the typical mean phonon-energy $h\bar{\nu}_v$ would directly change the slope of relation as shown in Supplementary Figure 4c.

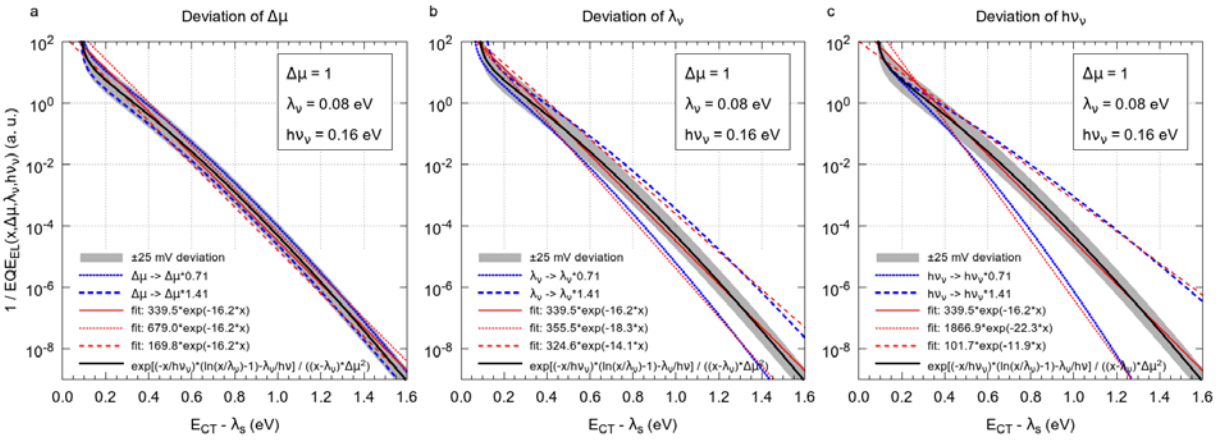


**Supplementary Figure 4 | Error Analyses for Approximating the Energy-Gap Law.** The Supplementary Equation (19) is simplified to Supplementary Equation (21) by assuming that $\Delta\mu$, $\lambda_v$, and $h\nu_v$ are rather constant for all investigated materials. **a-c** show a variation of each parameter by a factor of 2. The black curve represents the reciprocal of Supplementary Equation (19) for typical values, given in the upper right corner of the plot, and the grey area a corresponding variation of ±25 mV. The blue dashed lines correspond to reciprocal of Supplementary Equation (19) with the variation of one parameter by a total factor of 2. Red lines show exponential fits to the curves having the same line type.

In Figure 3a in the main text, we observe a trend where the $\Delta V_{nr}$ changes by about 255 mV from $x$ = (0.2 to 1.4) eV which equals a change of $EQE_{EL}$ by ~$3 \cdot 10^5$. The experimental data is scattered

which can be mainly explained by moderate deviations of $\Delta\mu$ and $\lambda_v$ which would mainly cause scattering in the height of single $\Delta V_{nr}$ values. However, the observation of a clear trend indicates that $h\bar{\nu}_v$ has to be quite constant over all molecules, otherwise a trend would not be visible.

## Supplementary Notes 3 - Impact of Intrinsic Non-Radiative Recombination on the Maximum *PCE* of OSCs

The Shockley-Queisser (SQ) or detailed balance limit for the *PCE* of a single junction SC with an optical gap $E_g$ makes the following assumptions[12]:

(i) Perfect absorption of photons with energy $E$ higher than the optical gap $E_g$, with each photon creating exactly one electron-hole pair. The absorption for photons with energy $E<E_g$ is zero.

(ii) Perfect separation and collection of charge carriers, i.e. perfect internal quantum efficiency (*IQE*), which requires mobility-times-lifetime products much larger than the device thickness and the absence of geminate recombination.

(iii) Radiative, i.e. non-geminate, recombination is the only allowed recombination mechanism. In other words, the $EQE_{EL}$ equals to one.

In what follows, we re-derive the SQ limit[12], and adjust it for OSCs. Point (i) and (ii) assume that $EQE_{PV}$ equals 100% for photon energies higher than $E_g$, while it is zero below $E_g$. With respect to this assumption, the maximum obtainable photocurrent under AM1.5G illumination with photon-flux spectrum $\varphi_{AM1.5}(E)$ can be calculated:

$$j_{ph}^{SQ}(E_g) = q\int_0^{+\infty} EQE_{PV}(E)\varphi_{AM1.5g}(E)\mathrm{d}E = q\int_{E_g}^{+\infty} \varphi_{AM1.5g}(E)\mathrm{d}E \ . \quad (22)$$

For inorganic SCs, such as GaAs and Si, $EQE_{PV}$ values well over 90% have been demonstrated. For OSCs, some D:A blends were demonstrated to have *IQE* values close to 100%[13], resulting in $EQE_{PV}$ values of about 80-90% above the optical gap $E_g$ of the main absorber. Therefore, the $j_{SC}$ is rather close to the theoretical maximum for both inorganic SCs and the best OSCs.

Due to assumption (iii) recombination occurs only via radiative recombination. Assuming the reciprocity between absorption and emission[14] and that the absorption is negligible below the optical gap (i) the recombination current density $j_{rec}(V)$ can be calculated:

$$j_{rec}(V) = j_0^{SQ}\left(\exp\left(\frac{qV}{k_BT}\right) - 1\right) \ , \quad (23)$$

with:

$$j_0^{SQ}(E_g,T) = q\int_0^{+\infty} EQE_{PV}(E)\,\varphi_{BB}(E,T)\mathrm{d}E = q\int_{E_g}^{+\infty} \varphi_{BB}(E,T)\mathrm{d}E \ , \quad (24)$$

with $\varphi_{\mathrm{BB}}(E,T)$ the black body spectrum. Since the total current density is the sum of $j_{\mathrm{ph}}$ and $j_{\mathrm{rec}}$, an expression for the current-voltage $j(V)$ relationship under the assumptions (i)-(iii) can be derived[12, 15, 16, 17]:

$$j(V) = j_0\left(\exp\left(\frac{qV}{k_{\mathrm{B}}T}\right)-1\right)-j_{\mathrm{ph}}\ . \tag{25}$$

The maximum $V_{\mathrm{OC}}$ is then given by:

$$V_{\mathrm{OC}}^{\mathrm{SQ}} = \frac{k_{\mathrm{B}}T}{q}\ln\left(\frac{j_{\mathrm{ph}}^{\mathrm{SQ}}}{j_0^{\mathrm{SQ}}}+1\right). \tag{26}$$

Our work shows that assumption (iii) is violated for OSCs, with $EQE_{\mathrm{EL}}$ being substantially lower than one, due to the presence of unavoidable intermolecular vibrational modes. Together with electron transfer losses, the additional non-radiative recombination results in a decreased $V_{\mathrm{OC}}$, which depends on $E_{\mathrm{g}}$:

$$V_{\mathrm{OC}}\left(E_{\mathrm{g}},\Delta(E_{\mathrm{g}})\right) = V_{\mathrm{OC}}^{\mathrm{SQ}}(E_{\mathrm{g}})-\Delta(E_{\mathrm{g}})\ . \tag{27}$$

For a *jV*-curve given by Supplementary Equation (25), the following recursive formulas relate the $V_{\mathrm{OC}}$ to the fill factor (*FF*):

$$FF = \frac{\left(\frac{qV_{\mathrm{MPP}}}{k_{\mathrm{B}}T}\right)^2}{\left(1+\frac{qV_{\mathrm{MPP}}}{k_{\mathrm{B}}T}-\exp\left(-\frac{qV_{\mathrm{MPP}}}{k_{\mathrm{B}}T}\right)\right)\left(\frac{qV_{\mathrm{MPP}}}{k_{\mathrm{B}}T}+\ln\left(1+\frac{qV_{\mathrm{MPP}}}{k_{\mathrm{B}}T}\right)\right)}\ , \tag{28}$$

with:

$$V_{\mathrm{OC}}\left(E_{\mathrm{g}},\Delta(E_{\mathrm{g}})\right) = V_{\mathrm{MPP}}+\frac{k_{\mathrm{B}}T}{q}\ln\left(1+\frac{qV_{\mathrm{MPP}}}{k_{\mathrm{B}}T}\right). \tag{29}$$

Now we have expressions for the maximum $j_{\mathrm{SC}}$, the $V_{\mathrm{OC}}$, and the *FF* which allows us to set an upper limit for the *PCE* as a function of $\Delta(E_{\mathrm{g}})$.

$$PCE\left(E_{\mathrm{g}},\Delta(E_{\mathrm{g}})\right) = j_{SC}(E_{\mathrm{g}})\cdot V_{OC}\left(E_{\mathrm{g}},\Delta(E_{\mathrm{g}})\right)\cdot FF\left(E_{\mathrm{g}},\Delta(E_{\mathrm{g}})\right) \tag{30}$$

If $\Delta$ equals zero, we are in the SQ limit. However, for OSCs we have to adjust the detailed balance limit, since $\Delta$ will never be negligible due to the intrinsic non-radiative recombination which follows the EGL. Since it has been shown that the electron transfer losses can be reduced to rather low values <50 meV, still keeping the *IQE* rather high[18, 2, 19, 20], these voltage losses do not seem to be fundamental. However, as we demonstrate in this work, the voltage losses due to non-radiative recombination are intrinsic, obeying an EGL with a simplified relation:

$$\Delta(E_{\mathrm{g}}) = \frac{k_{\mathrm{B}}T}{q}\ln\left(\frac{1}{EQE_{\mathrm{EL}}}\right) = A-B\cdot E_{\mathrm{g}}\ . \tag{31}$$

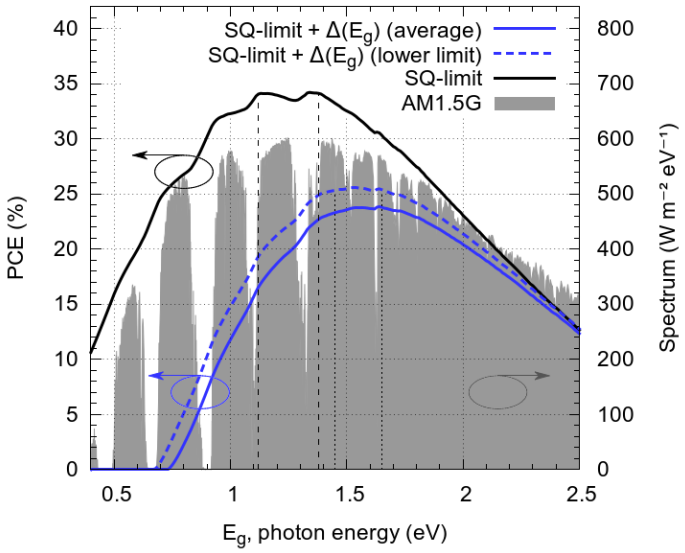


**Supplementary Figure 5 | Upper Limit for PCE as a Function of the Optical Gap and Additional Voltage Losses.** Maximum *PCE* of a single junction SC under the assumptions (i)-(iii) as a function of the optical gap ($E_g$), shown as solid black line. The maximum *PCE* of OSCs is reduced due to intrinsic non-radiative voltage losses $\Delta(E_g)$. The dashed blue line represents the minimal amount of intrinsic voltage losses which are found to be typical for OSCs, therefore, the highest, theoretical *PCE* for OSCs reduces to about 25.5%. The solid blue line shows the average losses obtained in this study. The intrinsic non-radiative voltage losses $\Delta(E_g)$ cause a blue-shift of the optimal optical gap ($E_g$), indicated by vertical dashed lines, from (1.12-1.38) eV to (1.45-1.65) eV. The filled grey curve represents the AM1.5G sun spectrum as a function of the photon energy.

Taking into account Supplementary Equation (31), we derive a corrected upper limit for the *PCE* of OSCs, shown in Supplementary Figure 5 as blue lines. *PCE*s below the doted blue line are in principle reachable, the limiting case is described by an $EQE_{PV}$ of 100% above the optical gap of the main absorber and no electron transfer losses. *PCE*s above the doted blue line are found to be not reachable for OSCs. The highest *PCE* of 25-26% is achieved for absorber molecules with an $E_g$ of (1.45-1.65) eV. The $V_{OC}$ for these devices with an optimized optical gap and assuming no electron transfer losses but following the EGL is accordingly (0.93-1.17) V.

One of the currently best OSCs[21] has an optical gap of about 1.65 eV, a $V_{OC}$ of 0.78 V, and an *FF* of 73% resulting in a *PCE* of 11.7%. This device has an $EQE_{PV}$ of 83-86%. If we could optimize the voltage of this device by decreasing the electron transfer losses, the unavoidable non-radiative losses would limit the possible *PCE* to about 17.6%.

Up to now, OSCs with an $EQE_{PV}$ of 85%[21] and *FF* of 80%[22] have been demonstrated. For an absorber with an optimal $E_g$, the maximum *PCE* for such a device would amount 19.5% by taking the intrinsic non-radiative voltage losses into account. This optimal $E_g$ is (1.52-1.54) eV, resulting in a maximal $V_{OC}$ of (1.01-1.04) V.

# Supplementary Tables

**Supplementary Table 2 | Overview of Used Donor Materials and Their Suppliers.**

| No. | Short Name | Chemical Structure | Long Name | Supplier |
|---|---|---|---|---|
| 1 | **2-TNATA** | 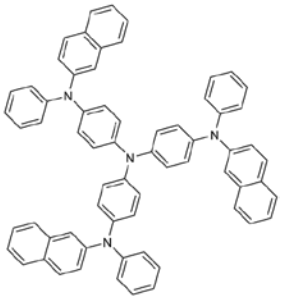 | 4,4',4''-tris(2-naphthylphenylamino)-triphenylamine | Sensient |
| 2 | **4P-TPD** | 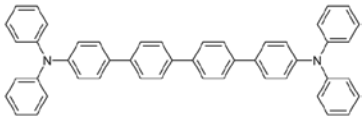 | 4,4'''-bis(*N,N*-ditphenylamino)-1,1':4',1'':4'',1'''-quaterphenyl | Sensient |
| 3 | **α-6T** | 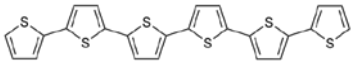 | 2,2':5',2'':5'',2''':5''',2'''':5'''',2''''':5''''',2''''''-sexithiophene | Lumtec |
| 4 | **BDTA-BT** | 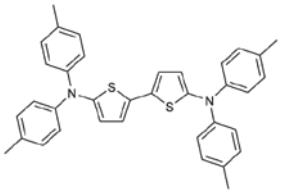 | 5,5'-bis(*N,N*-di-*p*-tolylamino)-2,2'-bithiophene | Georgia Institute of Technology |
| 5 | **BDTA-DTP** | 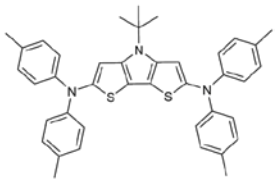 | *N*-(4-*tert*-butylphenyl)-2,6-bis(*N,N*-di-*p*-tolylamino)dithieno[3,2-*b*;2',3'-*d*]pyrrole | Georgia Institute of Technology |
| 6 | **BF-DPB** | 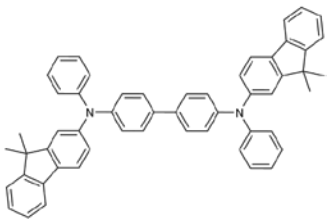 | *N,N'*-diphenyl-*N,N'*-bis(9,9-dimethyl-fluoren-2-yl)-benzidine | Synthon |
| 7 | **BPAPF** | 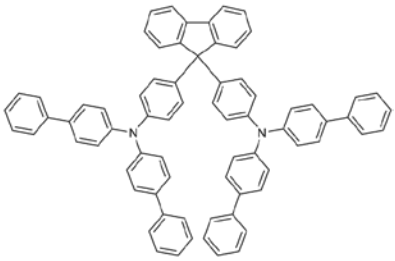 | 9,9-bis[4-(*N,N*-bis-biphenyl-4-yl-amino)phenyl]-9*H*-fluorene | Lumtec |

| | | | | |
|---|---|---|---|---|
| **8** | **BP-Bodipy** | 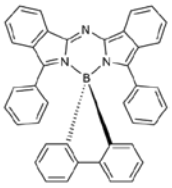 | 10',14'-diphenyl5λ$^4$,11'λ$^4$spiro[dibenzo[*b,d*]borole-5,12'-[1,3,5,2]1,3,5,2]triazaborinino[4,3-*a*:6,1-a']diisoindole] | TU Dresden |
| **9** | **DH4T** | 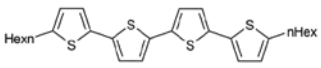 | 5,5'''-dihexyl-2,2':5',2'':5'',2''',2'''-quarterthiophene | University Ulm |
| **10** | **DH6T** | 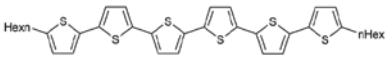 | 5,5''''-dihexyl-2,2':5',2'':5'',2''':5''',2'''':5'''',2'''''-sexithiophene | University Ulm |
| **11** | **DMFL-NPD** | 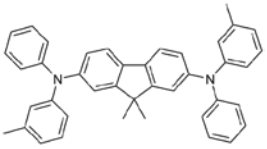 | 9,9-dimethyl-*N*,*N*'-diphenyl-*N*,*N*'-di-*m*-tolyl-9*H*-fluorene-2,7-diamine | Lumtec |
| **12** | **MeO-TPD** | 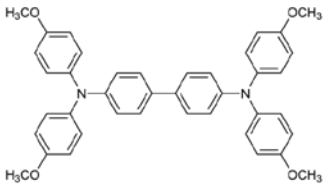 | *N*,*N*,*N*',*N*'-tetrakis(4-methoxyphenyl)-benzidine | Sensient |
| **13** | **m-MTDATA** | 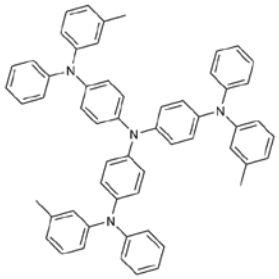 | 4,4',4''-tris(3-*m*-tolyl-phenylamino)-triphenylamine | Lumtec |
| **14** | **P4-Ph4-DIP** | 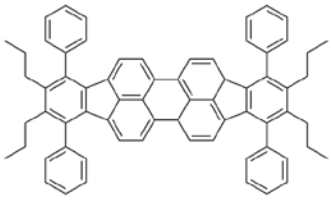 | 2,3,10,11-tetrapropyl-1,4,9,12-tetraphenyl-diindeno[1,2,3-*cd*:1',2',3'-*lm*]perylene | TU Dresden |
| **15** | **Rubrene** | 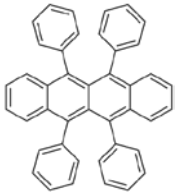 | 5,6,11,12-tetraphenyl-tetracene | Sensient |

| | | | | |
|---|---|---|---|---|
| **16** | **Rubrene $D_{28}$** | 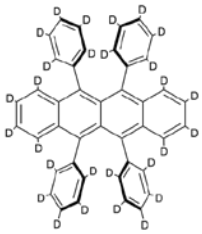 | 5,6,11,12-tetrakis (phenyl-$d_5$)tetracene-1,2,3,4,7,8,9,10-$d_8$ | University Minnesota Twin Cities |
| **17** | **Spiro-MeO-TAD** | 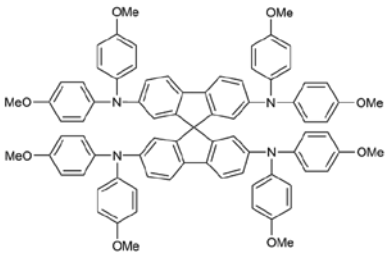 | 2,2',7,7'-tetrakis[*N,N*-di(4-methoxyphenyl) amino]-9,9'-spirobifluorene | Feiming Chemical Limited |
| **18** | **Spiro-MeO-TPD** | 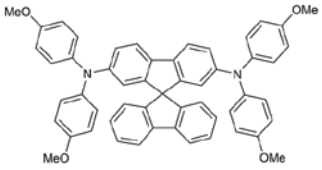 | 2,7-bis[*N,N*-bis(4-methoxy-phenyl) amino]9,9-spiro-bifluorene | Lumtec |
| **19** | **TAPC** | 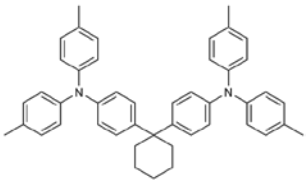 | 1,1-bis[4-(*N,N*-di-*p*-tolylamino)phenyl]cyclohexane | Sensient |
| **20** | **TCTA** | 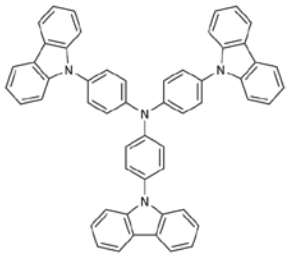 | 4,4',4''-tris(carbazol-9-yl)-triphenylamine | Sensient |
| **21** | **TPDP** | 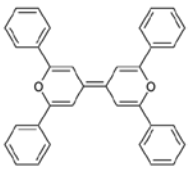 | 2,2',6,6'-tetraphenyl-4,4'-bipyranylidene | TU Dresden |
| **22** | **TPDP-Me** | 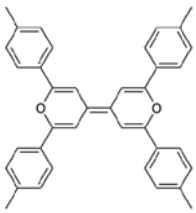 | 2,2',6,6'-tetra-*p*-tolyl-4,4'-bipyranylidene | TU Dresden |

| | | | | |
|---|---|---|---|---|
| **23** | **TPDP-OMe** | 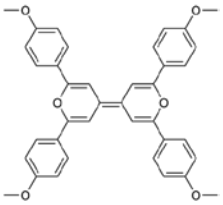 | 2,2',6,6'-tetrakis(4-methoxyphenyl)-4,4'-bipyranylidene | TU Dresden |
| **24** | **ZnPc** | 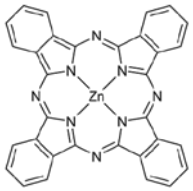 | zinc-phthalocyanine | CreaPhys GmbH |

**Supplementary Table 3 | Characteristic *jV*-Parameters of the Low-Donor-Content OSCs.** $C_{60}$ is the acceptor (94 mol%) and the donor was changed according to the list. The energy of the charge transfer (CT) state ($E_{CT}$) and the relaxation energy ($\lambda_s$) were obtained by fitting the low energy region of the sensitive $EQE_{PV}$ spectra which corresponds to the CT absorption. The corresponding error bars are obtained by a systematic variation of the fitting range. The ideal $V_{OC}$ under the assumption of only radiative recombination ($V_{OC,rad}$) was calculated from the $EQE_{PV}$ spectra, assuming the reciprocity relation between absorption and emission[1, 14]. The listed values correspond to illumination with simulated sunlight at an intensity of 1000 W/m$^2$.

| **Donor** | $j_{SC}$ (mA/cm$^2$) | ***FF*** (%) | ***PCE*** (%) | $V_{OC}$ (mV) | $V_{OC,rad}$ (mV) | $E_{CT}$ (meV) | $\lambda_s$ (meV) |
|---|---|---|---|---|---|---|---|
| 2-TNATA | 1.2 | 32 | 0.2 | 409 | 833 | 1011±1 | 417±13 |
| 4P-TPD | 5.3 | 51 | 2.7 | 990 | 1341 | 1576±4 | 187±13 |
| α-6T | 5.7 | 54 | 2.9 | 939 | 1269 | 1500±2 | 282±14 |
| BDTA-BT | 0.7 | 30 | 0.1 | 358 | 840 | 999±3 | 475±35 |
| BDTA-DTP | 0.3 | 31 | 0.01 | 108 | 630 | 751±10 | 532±77 |
| BF-DBP | 4.4 | 42 | 1.5 | 795 | 1131 | 1342±2 | 202±6 |
| BPAPF | 4.4 | 48 | 2.1 | 998 | 1318 | 1548±3 | 175±10 |
| BP-Bodipy | 6.8 | 49 | 2.9 | 870 | 1193 | 1453±1 | 125±4 |
| DH4T | 5.4 | 47 | 2.3 | 921 | 1291 | 1516±2 | 234±13 |
| DH6T | 5.6 | 49 | 2.5 | 897 | 1213 | 1444±2 | 281±19 |
| DMFL-NPD | 3.5 | 34 | 0.8 | 686 | 1062 | 1272±2 | 230±5 |
| MeO-TPD | 3.6 | 38 | 0.8 | 612 | 989 | 1195±2 | 193±8 |
| m-MTDATA | 1.1 | 32 | 0.1 | 358 | 787 | 954±1 | 407±16 |
| P4-Ph4-DIP | 5.6 | 46 | 2.6 | 1010 | 1373 | 1608±1 | 103±4 |
| Rubrene | 5.2 | 51 | 2.4 | 896 | 1243 | 1464±1 | 80±3 |
| Rubrene $D_{28}$ | 5.2 | 51 | 2.4 | 892 | 1244 | 1460±1 | 82±3 |

| | | | | | | | |
|---|---|---|---|---|---|---|---|
| Spiro-MeO-TAD | 2.4 | 34 | 0.5 | 568 | 953 | 1149±3 | 258±13 |
| Spiro-MeO-TPD | 3.0 | 33 | 0.5 | 527 | 939 | 1132±3 | 232±12 |
| TAPC | 5.2 | 58 | 2.7 | 907 | 1230 | 1448±1 | 159±6 |
| TCTA | 4.5 | 40 | 1.8 | 988 | 1313 | 1507±5 | 199±13 |
| TPDP | 0.8 | 40 | 0.1 | 256 | 761 | 913±1 | 164±5 |
| TPDP-Me | 0.7 | 39 | 0.04 | 165 | 698 | 821±1 | 146±7 |
| TPDP-OMe | 0.6 | 32 | 0.02 | 95 | 664 | 752±3 | 133±20 |
| ZnPc | 5.1 | 39 | 1.6 | 788 | 1103 | 1369±2 | 278±10 |

**Supplementary Table 4 | Information to Small Molecule OSCs.** The listed OSCs comprise D-A blends (mixing ratio is provided) or planar stacked of D and A. The energy of the charge transfer (CT) state ($E_{CT}$) was obtained by fitting the low energy region of the sensitive $EQE_{PV}$ spectra which corresponds to the CT absorption. The ideal $V_{OC}$ under the assumption of only radiative recombination ($V_{OC,rad}$) was calculated from the $EQE_{PV}$ spectra, using the reciprocity relation between absorption and emission[1, 14]. The *PCE* and the $V_{OC}$ correspond to illumination with simulated sunlight at an intensity of 1000 W/m$^2$.

| No. | Donor | Acceptor | Stoichiometry D:(D+A) (wt%) | *PCE* (%) | $V_{OC}$ (mV) | $V_{OC,rad}$ (mV) | $E_{CT}$ (meV) | Ref. |
|---|---|---|---|---|---|---|---|---|
| **BHJ (bulk heterojunction)** | | | | | | | | |
| 1 | α-6T | $C_{60}$ | 1 | 1.4 | 0.98 | 1.35 | 1.55 | - |
| 2 | α-6T | $C_{60}$ | 5 | 2.8 | 0.93 | 1.26 | 1.49 | - |
| 3 | α-6T | $C_{60}$ | 7 | 3.2 | 0.92 | 1.24 | 1.48 | - |
| 4 | α-6T | $C_{60}$ | 19 | 2.0 | 0.81 | 1.20 | 1.45 | - |
| 5 | α-6T | $C_{60}$ | 40 | 0.9 | 0.46 | 0.92 | 1.08 | - |
| 6 | α-6T | $C_{60}$ | 68 | 0.9 | 0.45 | 0.90 | 1.08 | - |
| 7 | BDTA-BT | $C_{60}$ | 10 | < 0.1 | 0.31 | 0.84 | 1.02 | - |
| 8 | BDTA-BT | $C_{60}$ | 20 | < 0.1 | 0.28 | 0.84 | 1.05 | - |
| 9 | BDTA-DTP | $C_{60}$ | 10 | < 0.1 | 0.04 | 0.59 | 0.73 | - |
| 10 | BDTA-DTP | $C_{60}$ | 20 | < 0.1 | 0.03 | 0.58 | 0.73 | - |
| 11 | BF-DPB | $C_{60}$ | 5 | 1.1 | 0.80 | 1.14 | 1.34 | - |
| 12 | BPAPF | $C_{60}$ | 5 | 1.3 | 1.00 | 1.33 | 1.55 | - |
| 13 | CNTF | $C_{60}$ | 50 | 1.2 | 0.88 | 1.15 | 1.47 | 23 |
| 14 | CNV301-5T | $C_{60}$ | 66 | 2.8 | 0.98 | 1.31 | 1.54 | - |
| 15 | CuPc | $C_{60}$ | 50 | 1.6 | 0.48 | 0.90 | 1.13 | - |
| 16 | $DCV_2$-4T | $C_{60}$ | 50 | 2.8 | 0.94 | 1.30 | 1.45 | - |
| 17 | $DCV_2$-4T | $C_{60}$ | 66 | 3.0 | 0.98 | 1.32 | 1.46 | 24 |
| 18 | $DCV_2$-4T-Et(1,1,4,4) | $C_{60}$ | 66 | 1.2 | 1.03 | 1.35 | 1.54 | - |
| 19 | $DCV_2$-5T-Me(1,1,5,5) | $C_{60}$ | 66 | 4.5 | 0.86 | 1.21 | 1.42 | 25 |
| 20 | $DCV_2$-5T-Me(2,2,4,4) | $C_{60}$ | 66 | 3.6 | 0.85 | 1.25 | 1.46 | 25 |

| | | | | | | | | |
|---|---|---|---|---|---|---|---|---|
| 21 | $DCV_2$-5T-Me(3,3) | $C_{60}$ | 66 | 6.9 | 0.96 | 1.25 | 1.47 | 26 |
| 22 | $DCV_2$-6T-Bu(1,2,5,6) | $C_{60}$ | 66 | 2.7 | 0.89 | 1.20 | 1.43 | - |
| 23 | DTDCTB | $C_{60}$ | 50 | 2.6 | 0.82 | 1.13 | 1.52 | - |
| 24 | $F_4$ZnPc | $C_{60}$ | 50 | 3.0 | 0.73 | 1.11 | 1.48 | - |
| 25 | $HAT(CN)_6$ | $C_{60}$ | 5 | 1.8 | 0.95 | 1.29 | 1.55 | - |
| 26 | m-MTDATA | $C_{60}$ | 5 | 0.8 | 0.38 | 0.80 | 0.97 | - |
| 27 | PRTF | $C_{60}$ | 50 | 2.4 | 0.90 | 1.16 | 1.48 | 23 |
| 28 | Spiro-MeO-TPD | $C_{60}$ | 5 | 0.9 | 0.55 | 0.95 | 1.13 | - |
| 29 | TAPC | $C_{60}$ | 1 | 1.1 | 0.92 | 1.28 | 1.46 | - |
| 30 | TAPC | $C_{60}$ | 10 | 2.3 | 0.87 | 1.21 | 1.44 | - |
| 31 | TAPC | $C_{60}$ | 20 | 1.4 | 0.83 | 1.19 | 1.45 | - |
| 32 | TAPC | $C_{60}$ | 50 | 0.1 | 0.76 | 1.19 | 1.46 | - |
| 33 | TFTF | $C_{60}$ | 50 | 1.3 | 0.82 | 1.14 | 1.47 | 23 |
| 34 | TPDP | $C_{60}$ | 20 | <0.1 | 0.13 | 0.69 | 0.89 | - |
| 35 | TPDP | $C_{60}$ | 33 | <0.1 | 0.08 | 0.65 | 0.85 | - |
| 36 | TPDP | $C_{60}$ | 50 | <0.1 | 0.03 | 0.64 | 0.83 | - |
| 37 | TPDP | $C_{60}$ | 66 | <0.1 | 0.07 | 0.68 | 0.88 | - |
| 38 | ZnF4Pc | $C_{60}$ | 50 | 0.6 | 0.89 | 1.21 | 1.54 | - |
| 39 | ZnPc | $C_{60}$ | 50 | 2.7 | 0.56 | 0.93 | 1.18 | - |
| **PHJ (planar heterojunction)** | | | | | | | | |
| 40 | BF-DPB | $C_{60}$ | PHJ | 1.1 | 0.74 | 1.13 | 1.31 | - |
| 41 | BPAPF | $C_{60}$ | PHJ | 1.3 | 0.93 | 1.27 | 1.46 | - |
| 42 | CuPc | $C_{60}$ | PHJ | 0.8 | 0.30 | 0.85 | 1.02 | - |
| 43 | DBP | $C_{60}$ | PHJ | 2.6 | 0.83 | 1.23 | 1.41 | - |
| 44 | ZnPc | $C_{60}$ | PHJ | 0.9 | 0.41 | 0.89 | 1.06 | - |

**Supplementary Table 5 | Information to Polymer OSCs.** The listed OSCs comprise D-A blend with polymeric donor molecules. The energy of the charge transfer (CT) state ($E_{CT}$) was obtained by fitting the low energy region of the sensitive $EQE_{PV}$ spectra which corresponds to the CT absorption. The ideal $V_{OC}$ under the assumption of only radiative recombination ($V_{OC,rad}$) was calculated from the $EQE_{PV}$ spectra, using the reciprocity relation between absorption and emission[1, 14]. The *PCE* and the $V_{OC}$ correspond to illumination with simulated sunlight at an intensity of 1000 W/m$^2$.

| No. | Donor | Acceptor | Stoichiometry D:(D+A) (wt%), comment | *PCE* (%) | $V_{OC}$ (mV) | $V_{OC,rad}$ (mV) | $E_{CT}$ (meV) | Ref. |
|---|---|---|---|---|---|---|---|---|
| The $EQE_{PV}$ spectra of published polymer OSCs were re-analysed with respect to their non-radiative voltage losses. Further details on the OSCs can be found in the corresponding reference. | | | | | | | | |
| 1 | $APFO_3$ | $PC_{61}BM$ | 20 | <0.5 | 1.05 | 1.38 | 1.64 | [1] |
| 2 | $APFO_3$ | $PC_{61}BM$ | 50 | ~2.0 | 1.08 | 1.46 | 1.66 | [27] |
| 3 | $APFO_3$ | $PC_{61}BM$ | 80 | ~4.0 | 1.16 | 1.48 | 1.66 | [27] |
| 4 | $APFO_3$ | $PC_{71}BM$ | 20 | <0.5 | 0.98 | 1.39 | 1.63 | [27] |
| 5 | $APFO_3$ | $PC_{71}BM$ | 50 | ~2.0 | 1.00 | 1.41 | 1.66 | [27] |
| 6 | Dihexyl-PTV | $PC_{61}BM$ | 50 | 0.5 | 0.57 | 1.02 | 1.22 | [28] |
| 7 | High-Tg-PPV | $PC_{61}BM$ | 20 | 1.0 | 0.82 | 1.20 | 1.44 | [28] |
| 8 | LBPP5 | $PC_{71}BM$ | 20 | ~3.0 | 0.73 | 1.14 | 1.39 | [27] |
| 9 | MDMO-PPV | $PC_{61}BM$ | 20 | 1.7 | 0.84 | 1.15 | 1.41 | [1] |
| 10 | MDMO-PPV | $PC_{61}BM$ | 50 | 0.7 | 0.88 | 1.22 | 1.47 | [28] |
| 11 | MDMO-PPV | $PC_{61}BM$ | 80 | <0.1 | 0.92 | 1.27 | 1.53 | [27] |
| 12 | MDMO-PPV | $PC_{61}BM$ | 90 | <0.1 | 0.91 | 1.27 | 1.53 | [28] |
| 13 | MDMO-PPV | $PC_{61}BM$ | 95 | <0.1 | 0.97 | 1.28 | 1.52 | [28] |
| 14 | OC9-PEO-PPV | $PC_{61}BM$ | 20 | 0.7 | 0.65 | 1.13 | 1.34 | [28] |
| 15 | P34T | $PC_{61}BM$ | 50, f=20% | ~1.0 | 0.49 | 0.97 | 1.18 | [29] |
| 16 | P34T | $PC_{61}BM$ | 50, f=51% | ~2.0 | 0.47 | 0.93 | 1.15 | [29] |
| 17 | P35T | $PC_{61}BM$ | 50, f=27% | ~2.0 | 0.57 | 0.99 | 1.21 | [29] |
| 18 | P35T | $PC_{61}BM$ | 50, f=38% | ~3.0 | 0.50 | 0.96 | 1.18 | [29] |
| 19 | P35T | $PC_{61}BM$ | 50, f=51% | ~3.0 | 0.50 | 0.95 | 1.17 | [29] |
| 20 | P35T | $PC_{61}BM$ | 50, f=63% | ~2.0 | 0.50 | 0.93 | 1.15 | [29] |
| 21 | P36T | $PC_{61}BM$ | 50, f=14% | ~3.0 | 0.63 | 1.06 | 1.24 | [29] |
| 22 | P36T | $PC_{61}BM$ | 50, f=34% | ~3.0 | 0.61 | 1.05 | 1.22 | [29] |
| 23 | P36T | $PC_{61}BM$ | 50, f=42% | ~3.0 | 0.60 | 1.05 | 1.21 | [29] |
| 24 | P36T | $PC_{61}BM$ | 50, f=49% | ~2.5 | 0.58 | 1.02 | 1.20 | [29] |
| 25 | P3HT | $PC_{61}BM$ | 50, as cast | 1.1 | 0.76 | 1.10 | 1.37 | [27] |
| 26 | P3HT | $PC_{61}BM$ | 50, annealed | 2.7 | 0.62 | 1.04 | 1.20 | [27] |
| 27 | ReRa-P3HT | $PC_{61}BM$ | 50 | 0.2 | 0.87 | 1.20 | 1.47 | [28] |
| 28 | PBDTTPD | $PC_{71}BM$ | 40 | 7.3 | 0.94 | 1.34 | 1.54 | [30] |
| 29 | PCDTBT | $PC_{71}BM$ | 25 | 4.1 | 0.87 | 1.26 | 1.48 | - |
| 30 | PCPDTBT | $PC_{71}BM$ | 33 | 2.5 | 0.67 | 1.05 | 1.29 | [27] |

| | | | | | | | | |
|---|---|---|---|---|---|---|---|---|
| 31 | PCPDTBT | $PC_{71}BM$ | 33, with ODT | 5.5 | 0.64 | 1.01 | 1.25 | 27 |
| 32 | TQm6 | $PC_{71}BM$ | 25 | 4.3 | 0.86 | 1.17 | 1.45 | 31 |
| 33 | TQm8 | $PC_{71}BM$ | 25 | 5.0 | 0.87 | 1.22 | 1.48 | 31 |
| 34 | TQmEH | $PC_{71}BM$ | 25 | 2.9 | 0.80 | 1.14 | 1.43 | 31 |
| 35 | TQp6 | $PC_{71}BM$ | 50 | 0.5 | 0.52 | 1.00 | 1.21 | 31 |
| 36 | TQp8 | $PC_{71}BM$ | 33 | 1.9 | 0.65 | 1.06 | 1.27 | 31 |
| 37 | TQp12 | $PC_{71}BM$ | 25 | 1.8 | 0.76 | 1.09 | 1.31 | 31 |
| Values which were taken from recent publications: | | | | | | | | |
| 38 | DTD | N2200 | 50 | 3.7 | 0.84 | 1.16 | 1.42 | 32 |
| 39 | PIPCP | $PC_{61}BM$ | 33 | 6.4 | 0.89 | 1.16 | 1.46[a] | 18 |
| 40 | PIDTT-TID | $PC_{71}BM$ | 25 | 6.7 | 1.00 | 1.24 | 1.57[b] | 20 |
| 41 | P3TEA | SF-$PDI_2$ | 40 | 9.5 | 1.37 | 1.37 | 1.72 | 2 |

**Supplementary Table 6 | Fit of $\Delta V_{nr}$ as a Function of ($E_{CT}$-$\lambda_s$) and of EL as a Function of the Photon-Energy.** The fit values corresponding to Figure 3a are listed for the trend obtained from $EQE_{PV}$ and $EQE_{EL}$. To compare the non-radiative voltage losses and the slope of the emission intensity, we apply the function $\frac{k_B T}{q}\ln(\text{emission}) = a + b \cdot \left(E - (E_{CT} - \lambda_s)\right)$, thus it follows $a = \frac{k_B T}{q}\ln(A')$ and $b = \frac{k_B T}{q} B$, in comparison to the fits applied in Supplementary Figure 6.

| ***x*-axis** (eV) | ***y*-axis** (mV) | **data set** | $y = a + b \cdot x$ | |
|---|---|---|---|---|
| | | | ***a* ± error *a*** (mV) | ***b* ± error *b*** (mV/eV) |
| $E_{CT}$ - $\lambda_s$ | $\Delta V_{nr}$ | low-donor | 574.3 ± 27.4 | -184.3 ± 25.8 |
| $E_{CT}$ - $\lambda_s$ | $\Delta V_{nr}$ | low-donor $EQE_{EL}$ | 556.1 ± 19.2 | -192.9 ± 16.3 |
| $E - (E_{CT} - \lambda_s)$ | $\frac{k_B T}{q}\ln(\text{emission})$ | selected EL spectra ($n$=10) | 8.8 ± 5.2 | 178.2 ± 22.2 |

[a] Consistently to our elaboration of the data, $E_{CT}$ should amount 1.46 eV. At this CT state energy both emission and absorption clearly cross.

[b] The $E_{CT}$ value was originally not provided in this publication. Here, $E_{CT}$ is obtained from the EL spectrum which is shown in the paper and is in good agreement with the $EQE_{PV}$ spectrum.

# Supplementary Figures

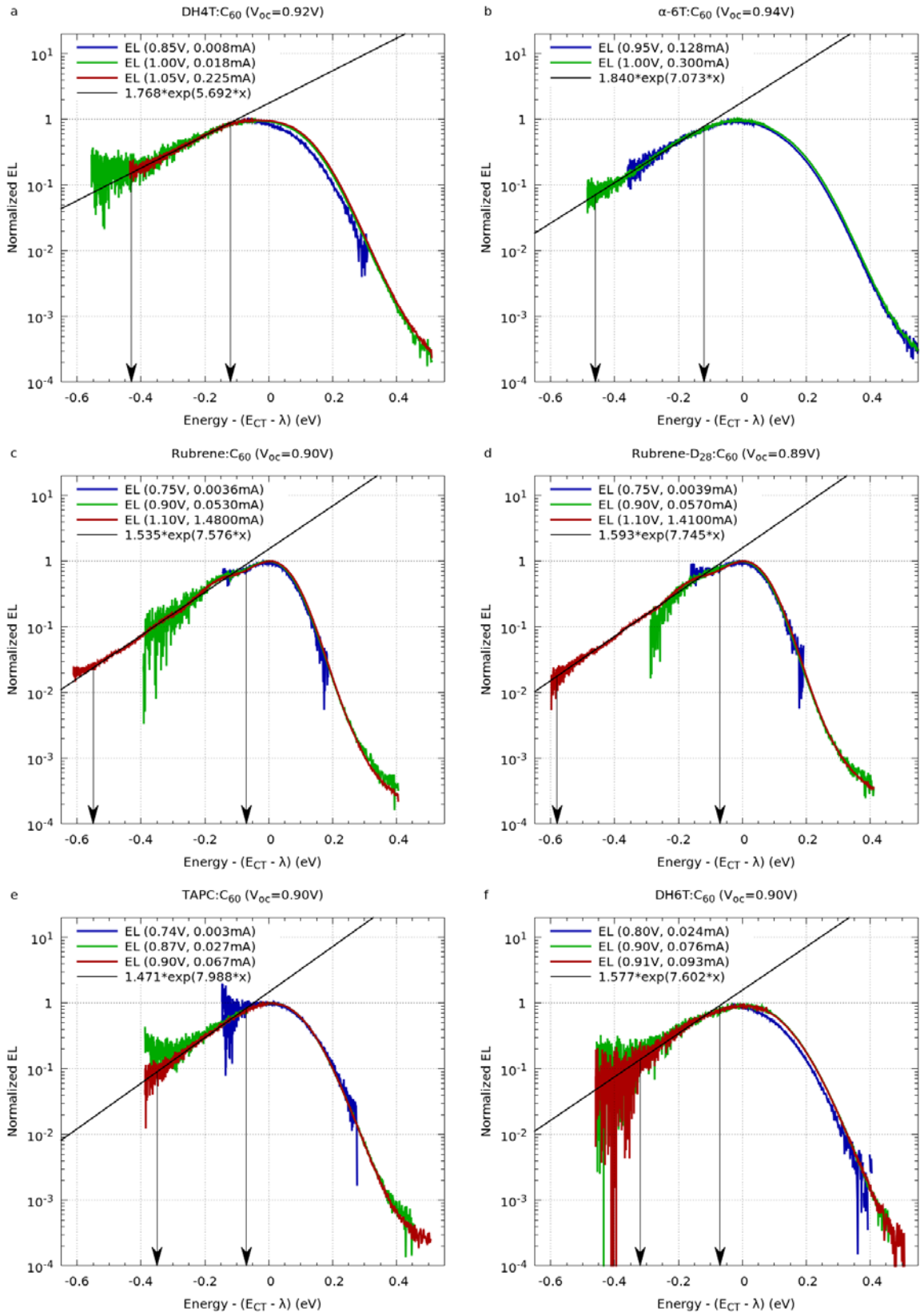

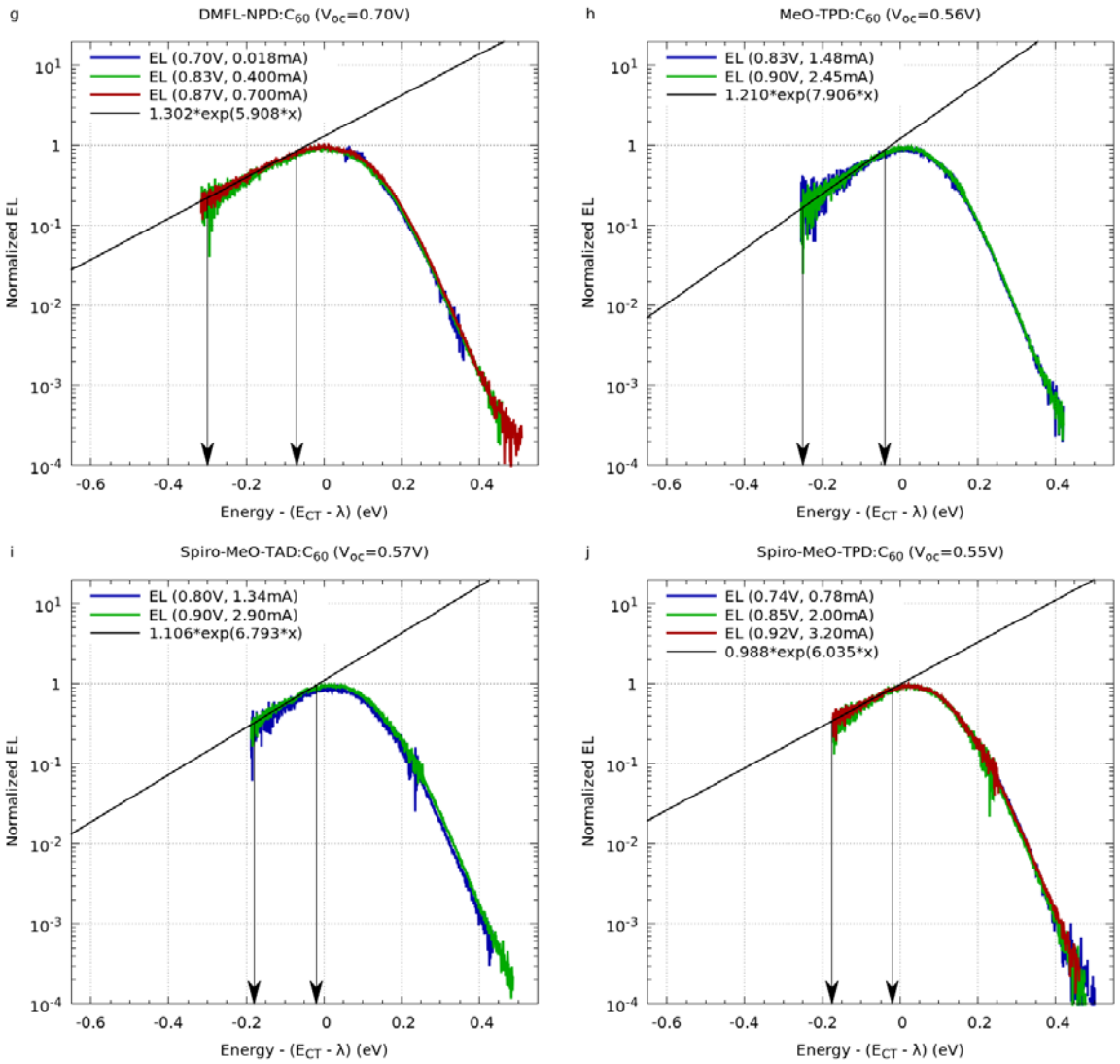


**Supplementary Figure 6 | Slope of the Low Energy CT State Emission.** Electroluminescence of different donor:$C_{60}$ CT states as a function of the photon-energy shifted by the peak of emission ($E_{CT} - \lambda_s$). The low energy tail is fitted by $y = A' \exp\left(B \cdot \left(E - \left(E_{CT} - \lambda_s\right)\right)\right)$. The *x*-range where the fit is applied is indicated by arrows. The low energy emission of all CT states has a similar slope (value of *B*).

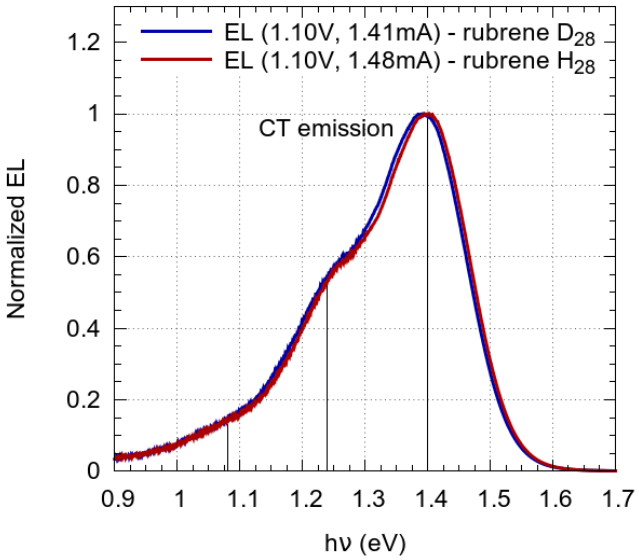


**Supplementary Figure 7 | CT State Emission of Rubrene and Deuterated Rubrene.** Electroluminescence of the CT state of $C_{60}$:rubrene and $C_{60}$:rubrene-$D_{28}$ as a function of the photon-energy. The low energy tail of the CT state emission for both D-A interfaces has the same sub-structure.

# Supplementary References


1. Vandewal, K., Tvingstedt, K., Gadisa, A., Inganäs, O. & Manca, JV., Relating the open-circuit voltage to interface molecular properties of donor:acceptor bulk heterojunction solar cells. *Phys Rev B* **81** (12), 125204 (2010).
2. Liu, J. *et al.*, Fast charge separation in a non-fullerene organic solar cell with a small driving force. *Nat Energy* **1** (9), 16089 (2016).
3. Vandewal, K., Interfacial Charge Transfer States in Condensed Phase Systems. *Annu Rev Phys Chem* **67** (February), 113-33 (2016).
4. Verhoeven, JW., Glossary of terms used in photochemistry (IUPAC Recommendations 1996). *Pure Appl Chem* **68** (12), 2223 (1996).
5. Väth, S. *et al.*, Triplet Excitons in Highly Efficient Solar Cells Based on the Soluble Small Molecule p-DTS(FBTTh2)2. *Adv Energy Mater* (1602016), 1-7 (2016).
6. Gould, IR., Farid, S. & Young, RH., Relationship Between Exciplex Fluorescence and Electron-Transfer in Radical Ion-Pairs. *J Photoch Photobio A* **65** (1-2), 133-147 (1992).
7. Gould, IR. *et al.*, Radiative and nonradiative electron transfer in contact radical-ion pairs. *Chem Phys* **176** (2-3), 439-456 (1993).
8. Vandewal, K. *et al.*, Charge-Transfer Absorption Tails of Photovoltaic Donor:C60 Blends Provide Insight into Thermally Activated Vibrations and Polaron Relaxation. *J Am Chem Soc* (139), 1699-1704 (2017).
9. Englman, R. & Jortner, J., The energy gap law for radiationless transitions in large molecules. *Mol Phys* **18** (2), 145-164 (1970).
10. Gould, IR. & Farid, S., Radiationless decay in exciplexes with variable charge transfer. *J Phys Chem B* **111** (24), 6782-6787 (2007).
11. Wilson, JS. *et al.*, The energy gap law for triplet states in Pt-containing conjugated polymers and monomers. *J Am Chem Soc* **123** (38), 9412-9417 (2001).
12. Shockley, W. & Queisser, HJ., Detailed balance limit of efficiency of p-n junction solar cells. *J Appl Phys* **32** (3), 510-519 (1961).
13. Vandewal, K. *et al.*, Efficient charge generation by relaxed charge-transfer states at organic interfaces. *Nat Mater* **13** (1), 63-68 (2013).
14. Rau, U., Reciprocity relation between photovoltaic quantum efficiency and electroluminescent emission of solar cells. *Phys Rev B* **76**, 1-8 (2007).
15. Green, M. A., General Temperature Dependence of Solar Cell Performance and Implications for Device Modelling. *Prog Photovoltaics* **11** (5), 333-340 (2003).
16. Dyer-Smith, C. & Nelson, J., in *Solar Cells - Material, Manufacture and Operation* (Elsevier B.V., Waltham, Amsterdam, Oxford, 2013), pp. 443-461.
17. Würfel, P. & Würfel, U., *Physics of Solar Cells*, 2nd ed. (WILEY-VCH Verlag, Weinheim, 2010).
18. Ran, NA. *et al.*, Harvesting the Full Potential of Photons with Organic Solar Cells. *Adv Mater* **28** (7), 1482-1488 (2016).
19. Vandewal, K. *et al.*, Quantification of Quantum Efficiency and Energy Losses in Low Bandgap Polymer:Fullerene Solar Cells with High Open-Circuit Voltage. *Adv Funct Mater* **22**, 3480-3490 (2012).

20. Wang, C. *et al.*, Low Band Gap Polymer Solar Cells with Minimal Voltage Losses. *Adv Energy Mat* **6** (18), 1600148 (2016).
21. Zhao, J. *et al.*, Efficient organic solar cells processed from hydrocarbon solvents. *Nat Energy* **1** (2), 15027 (2016).
22. Guo, X. *et al.*, Polymer solar cells with enhanced fill factors. *Nat Photonics* **7** (10), 825-833 (2013).
23. Fang, L. *et al.*, Thermally Stable Fluorine-Containing Low-Energy-Gap Organic Dyes with Low Voltage Losses for Organic Solar Cells. *Synthetic Met* **222**, 232-239 (2016).
24. Koerner, C. *et al.*, Probing the effect of substrate heating during deposition of DCV4T:C60 blend layers for organic solar cells. *Org Electron* **13** (4), 623-631 (2012).
25. Fitzner, R. *et al.*, Correlation of pi-conjugated oligomer structure with film morphology and organic solar cell performance. *J Am Chem Soc* **134** (27), 11064-11067 (2012).
26. Moench, T. *et al.*, Influence of Meso and Nanoscale Structure on the Properties of Highly Efficient Small Molecule Solar Cells. *Adv Energy Mater* **6** (4), 1-10 (2016).
27. Vandewal, K., Tvingstedt, K., Gadisa, A., Inganäs, O. & Manca, JV., On the origin of the open-circuit voltage of polymer-fullerene solar cells. *Nat Mater* **8** (11), 904-909 (2009).
28. Vandewal, K. *et al.*, The relation between open-circuit voltage and the onset of photocurrent generation by charge-transfer absorption in polymer:fullerene bulk heterojunction solar cells. *Adv Funct Mater* **18**, 2064-2070 (2008).
29. Vandewal, K. *et al.*, Varying polymer crystallinity in nanofiber poly(3-alkylthiophene): PCBM solar cells: Influence on charge-transfer state energy and open-circuit voltage. *Appl Phys Lett* **95** (12), 21-24 (2009).
30. Hoke, ET. *et al.*, Recombination in polymer:fullerene solar cells with open-circuit voltages approaching and exceeding 1.0 V. *Adv Energy Mater* **3** (2), 220-230 (2013).
31. Wang, E. *et al.*, Conformational disorder enhances solubility and photovoltaic performance of a thiophene-quinoxaline copolymer. *Adv Energy Mater* **3** (6), 806-814 (2013).
32. Tang, Z. *et al.*, A New Fullerene-Free Bulk-Heterojunction System for Efficient High-Voltage and High-Fill Factor Solution-Processed Organic Photovoltaics. *Adv Mater* **27** (11), 1900-1907 (2015).